doi:10.1093/brain/awab218 BRAIN 2021: 144; 3212–3225 | 3212

BRAIN
ORIGINAL ARTICLE

Dementia with Lewy bodies: association of Alzheimer pathology with functional connectivity networks

Julia Schumacher,[1,2] Jeffrey L. Gunter,[3] Scott A. Przybelski,[4] David T. Jones,[5] Jonathan Graff-Radford,[5] Rodolfo Savica,[5] Christopher G. Schwarz,[2] Matthew L. Senjem,[3] Clifford R. Jack Jr,[2] Val J. Lowe,[2] David S. Knopman,[5] Julie A. Fields,[6] Walter K. Kremers,[4] Ronald C. Petersen,[5] Neill R. Graff-Radford,[7] Tanis J. Ferman,[8] Bradley F. Boeve,[5] Alan J. Thomas,[1] John-Paul Taylor[1] and Kejal Kantarci[2]

Dementia with Lewy bodies (DLB) is neuropathologically defined by the presence of α-synuclein aggregates, but many DLB cases show concurrent Alzheimer's disease pathology in the form of amyloid-β plaques and tau neurofibrillary tangles.

The first objective of this study was to investigate the effect of Alzheimer's disease co-pathology on functional network changes within the default mode network (DMN) in DLB. Second, we studied how the distribution of tau pathology measured with PET relates to functional connectivity in DLB. Twenty-seven DLB, 26 Alzheimer's disease and 99 cognitively unimpaired participants (balanced on age and sex to the DLB group) underwent tau-PET with AV-1451 (flortaucipir), amyloid-β-PET with Pittsburgh compound-B (PiB) and resting-state functional MRI scans. The resing-state functional MRI data were used to assess functional connectivity within the posterior DMN. This was then correlated with overall cortical flortaucipir PET and PiB PET standardized uptake value ratio (SUVr). The strength of interregional functional connectivity was assessed using the Schaefer atlas. Tau-PET covariance was measured as the correlation in flortaucipir SUVr between any two regions across participants. The association between region-to-region functional connectivity and tau-PET covariance was assessed using linear regression. Additionally, we identified the region with highest and the region with lowest tau SUVrs (tau hot- and cold spots) and tested whether tau SUVr in all other brain regions was associated with the strength of functional connectivity to these tau hot and cold spots.

A reduction in posterior DMN connectivity correlated with overall higher cortical tau- ($r = –0.39$, $P = 0.04$) and amyloid-PET uptake ($r = –0.41$, $P = 0.03$) in the DLB group, i.e. patients with DLB who have more concurrent Alzheimer's disease pathology showed a more severe loss of DMN connectivity. Higher functional connectivity between regions was associated with higher tau covariance in cognitively unimpaired, Alzheimer's disease and DLB. Furthermore, higher functional connectivity of a target region to the tau hotspot (i.e. inferior/medial temporal cortex) was related to higher flortaucipir SUVrs in the target region, whereas higher functional connectivity to the tau cold spot (i.e. sensory-motor cortex) was related to lower flortaucipir SUVr in the target region.

Our findings suggest that a higher burden of Alzheimer's disease co-pathology in patients with DLB is associated with more Alzheimer's disease-like changes in functional connectivity. Furthermore, we found an association between the brain's functional network architecture and the distribution of tau pathology that has recently been described in Alzheimer's disease. We show that this relationship also exists in patients with DLB, indicating that similar mechanisms of connectivity-dependent occurrence of tau pathology might be at work in both diseases.

Received December 30, 2020. Revised March 19, 2021. Accepted April 22, 2021. Advance access publication June 11, 2021

1 Translational and Clinical Research Institute, Faculty of Medical Sciences, Newcastle University, UK
2 Department of Radiology, Mayo Clinic, Rochester, MN, USA
3 Department of Information Technology, Mayo Clinic, Rochester, MN, USA
4 Department of Quantitative Health Sciences, Mayo Clinic, Rochester, MN, USA
5 Department of Neurology, Mayo Clinic, Rochester, MN, USA
6 Department of Psychiatry and Psychology, Mayo Clinic, Rochester, MN, USA
7 Department of Neurology, Mayo Clinic, Jacksonville, FL, USA
8 Department of Psychiatry and Psychology, Mayo Clinic, Jacksonville, FL, USA

Correspondence to: Kejal Kantarci, MD, MS
Department of Radiology, Mayo Clinic, 200 First Street SW, Rochester, MN 55905, USA
E-mail: kantarci.kejal@mayo.edu

Keywords: Lewy body dementia; tau; amyloid; resting-state fMRI; PET

Abbreviations: DLB = dementia with Lewy bodies; DMN = default mode network; PiB = Pittsburgh compound-B; SUVr = standardized uptake value ratio

Introduction

Dementia with Lewy bodies (DLB) is the second most common form of neurodegenerative dementia after Alzheimer's disease[1] and is characterized by core clinical symptoms of visual hallucinations, cognitive fluctuations, parkinsonism and REM sleep behaviour disorder.[2] Neuropathologically, DLB is primarily defined by the presence of intracellular α-synuclein aggregates termed Lewy bodies.[3,4] However, many DLB cases also exhibit concurrent Alzheimer's disease pathology in the form of extracellular amyloid plaques and intraneuronal tau neurofibrillary tangles, which can be assessed at autopsy[5–7] or *in vivo* using PET imaging.[8,9] This additional pathological burden has been linked to higher atrophy rates in patients with DLB,[10–12] especially in the medial temporal lobe.[13] Clinically, coexisting Alzheimer's disease pathology in DLB is associated with a more severe manifestation of the disease,[14] a higher risk of institutionalization and mortality,[15,16] lower cognitive performance[17] and a more rapid cognitive decline.[6,11,18–20]

In Alzheimer's disease, the accumulation of tau pathology has been shown to follow a typical spatial pattern in autopsy studies[21,22] and on PET imaging[23–25] that appears to overlap with large-scale functional networks in the brain.[26–29] Similarly, amyloid pathology has been shown to preferentially accumulate in brain regions that are part of functional networks,[30] especially the default mode network (DMN).[31–34] The DMN is a network of spatially distinct brain regions that are activated in the absence of a specific task, but also during episodic memory processing and introspective tasks.[35,36] A decrease of connectivity within the posterior part of the DMN comprising the precuneus and posterior cingulate cortex has consistently been reported in patients with Alzheimer's disease compared to healthy ageing[37–40] and a loss of DMN connectivity has been linked to amyloid and tau pathology in Alzheimer's disease dementia and preclinical Alzheimer's disease.[26,33,41–43]

In DLB, results from functional connectivity studies are less consistent. In particular, it is not clear if and how the DMN is affected in DLB, with different studies showing increased,[44] decreased[45] or unchanged connectivity[46–49] within this network compared to control participants. Some of these inconsistent findings, especially with respect to DMN connectivity, might be explained by varying amounts of coexisting Alzheimer's disease pathology in different DLB cohorts.

The first aim of this study was therefore to investigate the effect of concurrent Alzheimer's disease pathology (amyloid and tau) on posterior DMN connectivity in patients with DLB. We hypothesized that a higher burden of Alzheimer's disease pathology in patients with DLB would be associated with a more severe loss of connectivity within the posterior DMN, i.e. a more Alzheimer's disease-like functional connectivity profile.

Several models have been suggested to explain the spreading and distribution of Alzheimer's disease pathology across the brain. One model that has attracted considerable attention is that of a prion-like spread where pathology is hypothesized to propagate trans-synaptically from neuron to neuron.[50–53] This hypothesis is supported by preclinical studies demonstrating that injection of tau aggregates into mouse brains leads to tau accumulation in brain regions that are spatially distinct, but synaptically connected to the injection site.[54,55]

Recent human PET imaging studies provide evidence for a spatial correspondence between regional prevalence of tau deposition and major functional networks in Alzheimer's disease.[26–29] Furthermore, it has been shown that regions that are more strongly functionally connected to the rest of the brain display more tau pathology in patients with Alzheimer's disease[56] and that functional connectivity rather than geometric distance best explains the spatial pattern of tau distribution in healthy ageing, Alzheimer's disease and vascular cognitive impairment.[57,58] In a longitudinal study, it has recently been shown that a combination of baseline tau levels and functional brain topology can be used to predict future rates of tau accumulation in Alzheimer's disease.[59] Taken together, these findings indicate that the distribution of tau pathology in Alzheimer's disease occurs along functional connectivity networks and might depend on the connectivity strength between regions.

The relationship between the distribution of tau pathology and functional connectivity in DLB remains an unanswered question despite the frequency of occurrence and clinical relevance of Alzheimer's disease pathology in this condition.[16] Therefore, the second aim of the present study was to investigate the relationship between tau deposition and functional network structure in patients with DLB. We hypothesized that, similar to Alzheimer's disease, the accumulation of tau pathology in DLB would be related to large-scale functional network structure.[26–29] Furthermore, we hypothesized that there would be an association of functional connectivity

between regions and the spatial pattern of tau-PET uptake in patients with DLB.[57]

Materials and methods

Participants

All participants included in this study were enrolled in the Mayo Clinic Rochester Alzheimer's Disease Research Center (ADRC, $n = 51$) or the Mayo Clinic Study of Aging (MCSA, $n = 101$). We selected participants who had a diagnosis of probable DLB according to consensus criteria[2,4] and had good quality resting-state functional MRI, structural MRI, AV-1451 (flortaucipir) tau-PET and Pittsburgh compound-B (PiB) amyloid-PET scans available ($n = 27$). Four of these patients with DLB had received a diagnosis of mild cognitive impairment with DLB core clinical features (MCI-LB) at their initial visit and a diagnosis of DLB at follow-up. Patients with an initial MCI-LB diagnosis who did not have follow-up confirmation of conversion to DLB were not included. As a comparison group, we included patients with Alzheimer's disease dementia ($n = 26$) from the ADRC and MCSA cohorts who were balanced on age and sex to the DLB cohort. The diagnosis of Alzheimer's disease dementia was made in accordance with National Institute on Aging-Alzheimer's Association Criteria[60] and all Alzheimer's disease dementia participants had high uptake on PiB PET (i.e. PiB-positive). Furthermore, 99 cognitively unimpaired participants from the MCSA were included as a control group.

Dementia severity was assessed using the Mattis Dementia Rating Scale (DRS) and the Clinical Dementia Rating Scale (CDR). The severity of parkinsonism was measured using the Unified Parkinson's Disease Rating Scale part III (UPDRS-III). Cognitive fluctuations were considered to be present if a patient scored 3 or 4 on the four-item Mayo Fluctuations Scale.[61] Visual hallucinations were characterized by being fully formed and recurrent, and not related to other medical factors, medications or advanced dementia. Probable REM sleep behaviour disorder was assessed by the Mayo Sleep Questionnaire.[62]

The study was approved by the Mayo Clinic Institutional Review Board and followed the Health Insurance Portability and Accountability Act (HIPAA) guidelines. All participants and their legally authorized representatives (for those with dementia), provided written informed consent before study participation.

PET acquisition

PET images were acquired on a PET/CT scanner (GE Healthcare) operating in 3D mode. Participants were injected with an average of 596 MBq (range 292–729) of ^{11}C-PiB, and following a 40-min ^{11}C-PiB uptake period, a 20-min PiB scan consisting of four 5-min dynamic frames was obtained. In a different session, participants were injected with an average of 370 MBq (range 333–407) of ^{18}F-AV-1451 (flortaucipir), and a 20-min flortaucipir PET scan consisting of four 5-min frames was obtained after 80 min of uptake.

MRI acquisition

MRI was performed on a 3 T GE scanner. Structural images were acquired with a magnetization prepared rapid gradient echo sequence, repetition time = 2300 ms, echo time = 3 ms, T1 = 900 ms, 8° flip angle, 26 cm field of view, 256 × 256 in-plane matrix with a phase field of view of 0.94 and slice thickness of 1.2 mm.

Resting-state functional MRI data were acquired using an eight-channel head coil, gradient echo planar image, repetition time = 3000 ms, echo time = 30 ms, 90° flip angle, 21 cm field of view, 64 × 64 in-plane matrix, slice thickness 3.3 mm without gap and 160 volumes were obtained. Participants were asked to keep their eyes open during the scan. All included functional MRI datasets showed <3 mm of translational movement, $<3°$ of rotational movement and passed visual inspection for artefacts.

PET preprocessing

PET images were analysed using a fully automated image processing pipeline.[63] Each PET was registered (rigid) to that participant's corresponding T_1-weighted structural MRI using SPM12. We segmented each MRI using SPM12 Unified Segmentation,[64] and computed non-linear deformation parameters between it and the Mayo Clinic Adult Lifespan Template (MCALT[65]; https://www.nitrc.org/projects/mcalt/) using ANTs.[66] We used these parameters to transform the MCALT_ADIR122 and Schaefer atlases[67] to determine regional cortical uptake of flortaucipir and PiB. Voxels whose estimated probability of being CSF was greater than being grey or white matter were excluded from the analysis.

The global cortical PiB retention standardized uptake value ratio (SUVr) was obtained from bilateral parietal (including posterior cingulate and precuneus), temporal, prefrontal, orbitofrontal and anterior cingulate regions, referenced to the median cerebellar grey matter uptake. High uptake on PiB (PiB-positive) was defined as a PiB PET SUVr of $\geqslant 1.48$.[68]

Flortaucipir SUVr in each voxel was calculated by referencing to the median value of right and left cerebellar crus uptake. High uptake on flortaucipir (flortaucipir-positive) was defined as a flortaucipir PET SUVr of $\geqslant 1.25$.[68,69]

For the first part of the analysis, the average flortaucipir and PiB SUVr of all cortical regions from the ADIR122 atlas was used as a measure of overall cortical flortaucipir and PiB uptake, respectively.[9]

Functional MRI preprocessing

The first three volumes of the functional MRI time series were removed and each voxel's time series was despiked using AFNI's 3dDespike program.[70] Slice-timing correction was then performed in SPM12 (https://www.fil.ion.ucl.ac.uk/spm/) followed by two-pass realignment to the mean functional image. Structural T_1-weighted images were co-registered to the functional image. Subsequently, unified segmentation and normalization to the template space was performed. The subject-space CSF and white matter segmentations were binarized at a probability threshold of 0.9 and eroded by two voxels in each direction to create an anatomically-based noise region of interest to be used in a component-based noise correction.[71] Voxel-wise time series were extracted from this region of interest and a principal component analysis was applied. The first six principal components were combined with the six motion parameters and their first temporal derivatives to form a nuisance regressor matrix (18 regressors in total). As a last step, AFNI's 3dBandpass function was used to simultaneously detrend, band-pass filter (0.009–0.08 Hz), and perform nuisance regression using the nuisance regressor matrix. Simultaneous filtering and nuisance regression avoids spectral misspecification of motion artefacts further reducing the impact of motion confounds.[72]

Assessment of posterior default mode network connectivity

For the first part of the analysis, connectivity within the posterior part of the DMN (pDMN) was calculated.[43,73] The high-dimensional independent component of interest that was used for the calculation of posterior DMN connectivity was extracted from the MCSA

Functional Connectivity Atlas[74] and transformed into individual subject space using the inverse warps created during preprocessing. A spatial-temporal regression was then performed with the component of interest using functions from the group independent component analysis of functional MRI (GIFT) toolbox,[75] yielding subject-specific representations of posterior DMN connectivity.

Assessment of region-to-region functional connectivity

For the second part of the analysis, region-to-region functional connectivity was assessed using 100 regions from the Schaefer functional MRI atlas, which provides a functional parcellation of the cortex (Fig. 1A).[67] To this end, the Schaefer atlas was transformed into individual subject space using the inverse ANTs warps created during preprocessing. The functional MRI data were then parcellated into 100 cortical regions based on this atlas and mean time series from each atlas region were extracted (Fig. 1B). Functional connectivity between regions was assessed by calculating Pearson's correlations between time series for each pair of regions, resulting in a 100 × 100 functional connectivity matrix for each participant. Correlation values were subsequently converted to z-scores using Fisher *r*-to-z transformation and auto-correlations were set to zero. Finally, group-average functional connectivity matrices were computed for each diagnostic group (cognitively unimpaired, Alzheimer's disease dementia and DLB).

To test whether the results were influenced by the specific choice of atlas parcellation, we repeated all analyses using the 400-region parcellation of the Schaefer atlas.

Assessment of tau covariance

Similar to the functional MRI data, the flortaucipir SUVr images were parcellated into 100 cortical regions using the same Schaefer atlas and mean flortaucipir SUVr for each atlas region was extracted for each participant (Fig. 1C). To assess tau covariance, for each atlas region, the mean flortaucipir SUVrs from all participants within one diagnostic group were collated into a vector (Fig. 1C). These flortaucipir SUVr vectors were then correlated between each pair of regions using Spearman's correlations.[57] Spearman's correlations were chosen specifically to avoid the estimation of tau covariance to be influenced by extreme flortaucipir SUVr values in certain regions or participants.[57] This resulted in a 100 × 100 tau-PET covariance matrix for each group (cognitively unimpaired, Alzheimer's disease dementia and DLB) where each entry indicates the similarity in flortaucipir uptake for a given pair of regions across participants. This approach has been widely applied to estimate grey matter[76,77] and metabolic covariance networks[78] and has previously been applied to flortaucipir images in Alzheimer's disease.[57] Similar to the functional connectivity matrices, the tau covariance matrices were converted to z-scores using Fisher *r*-to-z transformation and auto-correlations were set to zero.

Network-specificity of flortaucipir uptake

The regions from the Schaefer atlas have previously been grouped into seven large-scale functional networks based on clustering of an average functional connectivity matrix estimated from a large set of healthy control participants.[67] The seven networks include the fronto-parietal network, DMN, dorsal attention network, limbic network, ventral attention network, somatomotor network and visual network.[79] This was used to assess the network-specificity of flortaucipir uptake in Alzheimer's disease dementia and DLB.[28,30] To this end, mean z-scores within each region were calculated for each patient using the mean and standard deviation (SD) from the control group as reference values: z-score = (individual value − control mean)/control SD. The specificity of flortaucipir uptake for each functional network was then quantified using two metrics. First, individual z-score values were averaged across all regions belonging to one network, reflecting the degree of flortaucipir uptake within each network compared to the control group. Second, a goodness-of-fit analysis was performed on the z-scores to quantify the spatial correspondence between cortex-wide flortaucipir uptake and the functional network topology. Goodness-of-fit values were calculated as the difference between the mean z-score within a given network and the mean z-score of all regions outside the network.

Statistics

Statistical analyses were performed in R (https://www.r-project.org/) and MATLAB (v.R2018a). The connectivity of the posterior DMN and log-transformed overall cortical flortaucipir and PiB SUVr (from the ADIR122 atlas) were compared between the cognitively unimpaired, Alzheimer's disease dementia and DLB groups using univariate ANOVA with *post hoc* tests, Bonferroni-corrected for multiple comparisons. Furthermore, two-sample *t*-tests were applied to compare posterior DMN connectivity and overall cortical flortaucipir SUVr between PiB-positive and PiB-negative patients with DLB (uncorrected for multiple comparisons). Similarly, pDMN connectivity and overall cortical PiB SUVr were compared between flortaucipir-positive and flortaucipir-negative patients with DLB (uncorrected for multiple comparisons).

Correlations between overall cortical flortaucipir and PiB SUVrs and posterior DMN connectivity were assessed using Pearson's correlations in each diagnostic group separately.

The significance of the network-specificity of flortaucipir uptake was assessed by performing one-sample *t*-tests on the mean z-scores and on the goodness-of-fit values for each network, in the Alzheimer's disease dementia and DLB groups separately. *P*-values were Bonferroni-corrected across the seven networks.

The association between region-to-region functional connectivity and tau-PET covariance was assessed using linear regression with the group-average functional connectivity matrix as the independent variable and the tau covariance matrix as the dependent variable, separately in each diagnostic group. To test whether the results in the DLB group were mainly driven by PiB-positive patients, we repeated this analysis in the DLB PiB-positive and the DLB PiB-negative subgroups separately.

To test whether associations between functional connectivity and tau covariance were driven by spatial proximity between regions, we repeated the regression analysis while controlling for Euclidean distance between regions. Euclidean distance between any two regions *i and j* was calculated according to the following formula:

$$\text{Distance}_{ij} = \sqrt{(i_x - j_x)^2 + (i_y - j_y)^2 + (i_z - j_z)^2} \quad (1)$$

where $i_{x,y,z}$ and $j_{x,y,z}$ are the MNI coordinates of the centroids of the respective regions.

In accordance with the idea that tau propagation is a function of both the level of tau pathology in a region and the strength of connectivity between that region and a target region,[57] we hypothesized that regions that show high functional connectivity to regions with high levels of flortaucipir uptake, should also exhibit higher flortaucipir uptake. In contrast, regions that are strongly connected to regions with lower flortaucipir uptake, should themselves have lower flortaucipir uptake. To test this

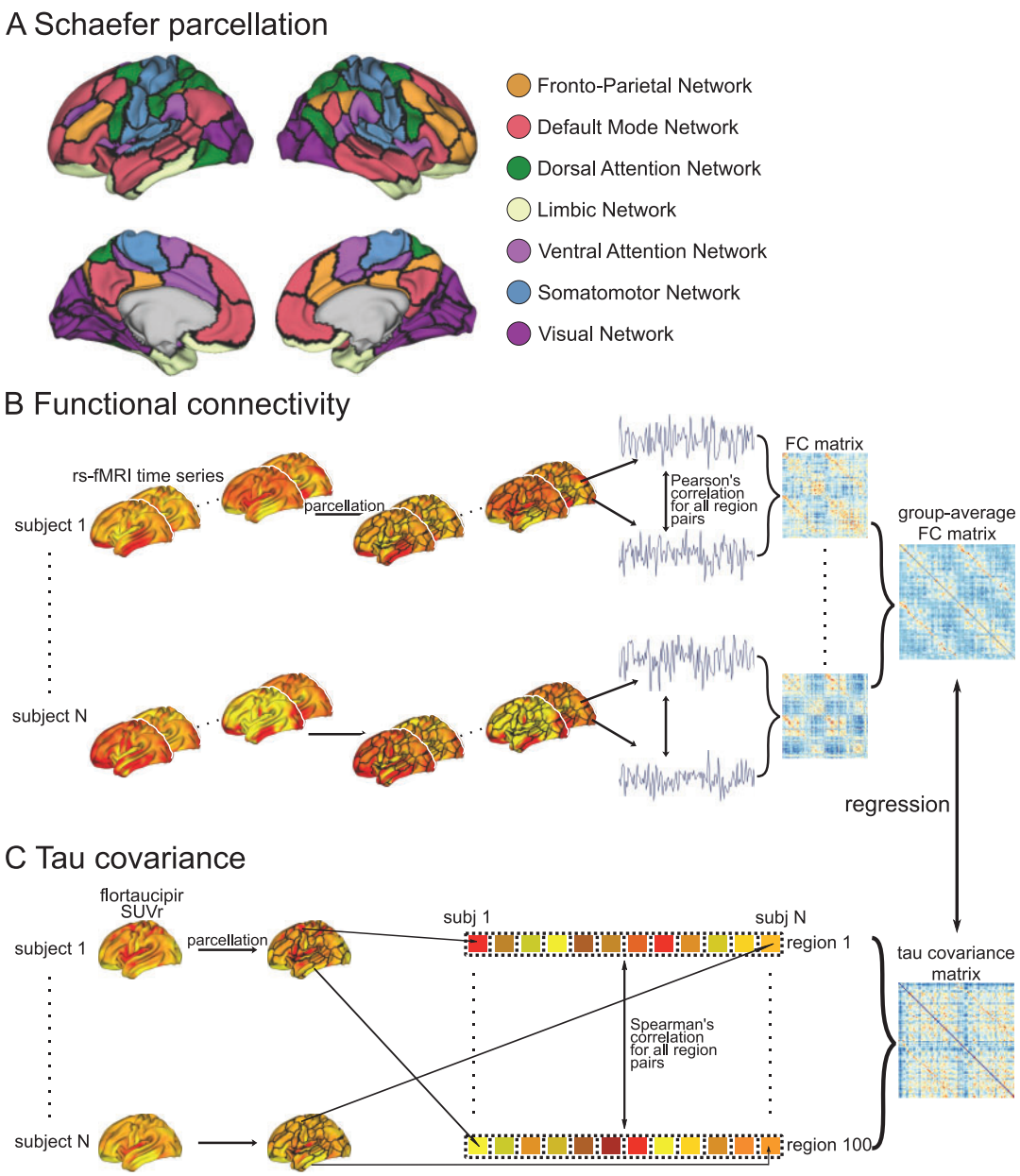

Figure 1 Functional MRI and PET analysis methods. (**A**) Schaefer functional parcellation that was used for parcellating flortaucipir SUVr and resting state functional MRI (rs-fMRI) images into 100 regions[67] and correspondence with the seven functional networks from Yeo *et al.*[79] (**B**) Functional connectivity analysis. (**C**) Tau covariance analysis. FC = functional connectivity.

hypothesis, for a given seed region, the group-average flortaucipir SUVrs of all other regions (target regions) were regressed onto the group-average functional connectivity values between the seed and the target regions. This was performed separately in each diagnostic group and was repeated for all regions (i.e. each region acted as a seed region once), resulting in a distribution of β-values for each group. Negative β-values indicate that higher seed-to-target connectivity is associated with lower flortaucipir uptake in the target region. In contrast, positive β-values indicate that higher seed-to-target connectivity is associated with higher flortaucipir uptake in the target region. To assess the association between a region's functional connectivity profile and flortaucipir uptake in the target regions, Pearson's correlations were calculated between flortaucipir SUVr in the seed region and the corresponding β-value, across all regions. This analysis was also repeated for the DLB PiB-positive and DLB PiB-negative subgroups separately.

To illustrate this relationship for the extreme cases, we identified the region with highest flortaucipir SUVr (tau hotspot) and the region with lowest flortaucipir SUVr (tau cold spot) for each diagnostic group.[57] We then tested whether tau SUVr in all other brain regions was associated with the strength of functional connectivity to these tau hot and cold spots by performing linear regression analyses. This analysis was performed in each diagnostic group and in the DLB PiB-positive and DLB PiB-negative subgroups separately.

To ensure that these results were not influenced by regions with very low flortaucipir uptake in the cognitively unimpaired and DLB groups, we selected only regions with flortaucipir SUVr >1.0 and >1.1 and repeated the analysis.

Furthermore, to assess whether PiB and *APOE* ε4 carrier status had any influence on these results in the DLB group we conducted the following analysis. The tau hot and cold spots were determined for each patient individually and the regression analysis between functional connectivity strength with the hot/cold spots and flortaucipir SUVr in the target regions was performed in each patient separately. The resulting distribution of β-values was tested for significance with a one-sample *t*-test to confirm that this relationship was significant at the single-participant level. Subsequently, two-sample *t*-tests were used to compare the resulting β-values between the DLB subgroups (DLB PiB-positive versus DLB PiB-negative and DLB *APOE* ε4 carriers versus DLB *APOE* ε4 non-carriers).

Data availability

The data that support the findings of this study are available from the corresponding author on reasonable request.

Results

Demographics

All three diagnostic groups were similar in age due to matching (Table 1). Since most DLB participants were male, the two comparison groups (Alzheimer's disease dementia and cognitively unimpaired) were selected so that they primarily included males. There was a higher percentage of *APOE* ε4 carriers in the Alzheimer's disease dementia group, but no significant difference in *APOE* ε4 status between DLB and cognitively unimpaired. Measures of functional (CDR sum of boxes) and cognitive (Mattis DRS) disease severity were not significantly different between Alzheimer's disease dementia and DLB. Most patients with DLB had parkinsonism and REM sleep behaviour disorder, 72% experienced cognitive fluctuations and 60% had visual hallucinations. Global cortical PiB SUVr and flortaucipir SUVr were higher in DLB compared to control participants and higher in Alzheimer's disease dementia compared to DLB. In the DLB group, there were 15 PiB-positive and 12 PiB-negative, and 11 flortaucipir-positive and 16 flortaucipir-negative participants. All patients with Alzheimer's disease dementia were PiB-positive and flortaucipir-positive.

For all included participants, the time between acquisition of functional MRI and PET data was <3 months. There was no significant difference between the groups in terms of time between the two scans [median days (range), cognitively unimpaired: 2 (0–63), Alzheimer's disease dementia: 1 (0–6), DLB: 2 (0–91); Kruskal–Wallis ANOVA, $F(2,149) = 2.2$, $P = 0.34$].

Association between default mode network connectivity and flortaucipir and PiB uptake

There was an overall group difference in posterior DMN connectivity [$F(2,149) = 9.9$, $P < 0.001$; Fig. 2A] with lower mean posterior DMN connectivity in the Alzheimer's disease dementia group compared to control participants ($P < 0.0001$) and compared to the DLB group ($P = 0.003$), but no significant difference between the DLB and control groups ($P = 0.96$).

There was a group difference in overall mean cortical flortaucipir SUVr [$F(2,149) = 140.8$, $P < 0.001$; Fig. 2B] with *post hoc* tests showing that overall uptake was higher in Alzheimer's disease dementia compared to control participants ($P < 0.001$) and in Alzheimer's disease dementia compared to DLB ($P < 0.001$), but not significantly different between DLB and control participants ($P = 0.70$). Overall cortical flortaucipir SUVr was marginally higher in PiB-positive compared to PiB-negative patients with DLB [$t(25) = 2.0$, $P = 0.053$].

There was a group difference in overall mean cortical PiB SUVr [$F(2,149) = 66.7$, $P < 0.001$; Fig. 2C] with *post hoc* tests showing that overall uptake was higher in Alzheimer's disease dementia compared to control participants ($P < 0.001$), in Alzheimer's disease dementia compared to DLB ($P < 0.001$) and in DLB compared to control participants ($P = 0.02$). Overall cortical PiB SUVr was higher in flortaucipir-positive compared to flortaucipir-negative patients with DLB [$t(25) = 3.9$, $P < 0.001$].

There was a significant correlation between posterior DMN connectivity and overall mean cortical flortaucipir SUVr in the DLB group ($r = –0.39$, $P = 0.04$), while this was marginally significant in the Alzheimer's disease dementia group ($r = –0.35$, $P = 0.08$) and

Table 1 Characteristics by diagnostic group

	CU *n* = 99 Data A	ADdem *n* = 26 Data B	DLB *n* = 27	CU-DLB *P*-value	ADdem-DLB *P*-value
Age, years	69.0 (10.3)	69.0 (7.3)	69.6 (7.1)	0.78	0.78
Male, *n* (%)	92 (93%)	23 (88%)	24 (89%)	0.49	0.96
APOE ε4 carrier, *n* (%)	27 (28%)	22 (88%)	10 (37%)	0.37	<0.001
CDR sum of boxes	0.1 (0.3)	5.7 (3.3)	4.6 (2.9)		0.21
DRS	NA	111.3 (21.0)	120.8 (22.6)		0.18
UPDRS	NA	1.6 (3.5)	18.1 (11.6)		<0.001
Disease duration	NA	5.7 (3.5)	6.6 (3.3)		0.36
Visual hallucinations, *n* (%)	NA	1 (4%)	15 (60%)		<0.001
Fluctuations, *n* (%)	NA	2 (8%)	18 (72%)		<0.001
Parkinsonism, *n* (%)	NA	3 (12%)	23 (92%)		<0.001
RBD, *n* (%)	NA	4 (15%)	24 (96%)		<0.001
PiB SUVr	1.50 (0.34)	2.48 (0.38)	1.73 (0.46)	0.003	<0.001
Flortaucipir SUVr	1.20 (0.11)	1.99 (0.32)	1.25 (0.12)	0.021	<0.001
PiB-positive, *n* (%)	28 (28%)	26 (100%)	15 (56%)	0.008	<0.001
Flortaucipir-positive, *n* (%)	26 (26%)	26 (100%)	11 (41%)	0.14	<0.001

Data are presented as mean (SD) for the continuous variables and *n* (%) for the categorical variables. *P*-values for differences between groups come from a *t*-test for the continuous variables or a chi-squared test for the categorical variables. PiB SUVr and flortaucipir SUVr were analysed with a log transformation. ADdem = Alzheimer's disease dementia; CDR = Clinical Dementia Rating Scale; CU = cognitively unimpaired; DLB = probable dementia with Lewy bodies; DRS = Mattis Dementia Rating Scale; flortaucipir-positive = flortaucipir PET SUVr of ⩾1.25; PiB-positive = PiB PET SUVr of ⩾1.48; RBD = REM sleep behaviour disorder; UPDRS = Unified Parkinson's Disease Rating Scale.

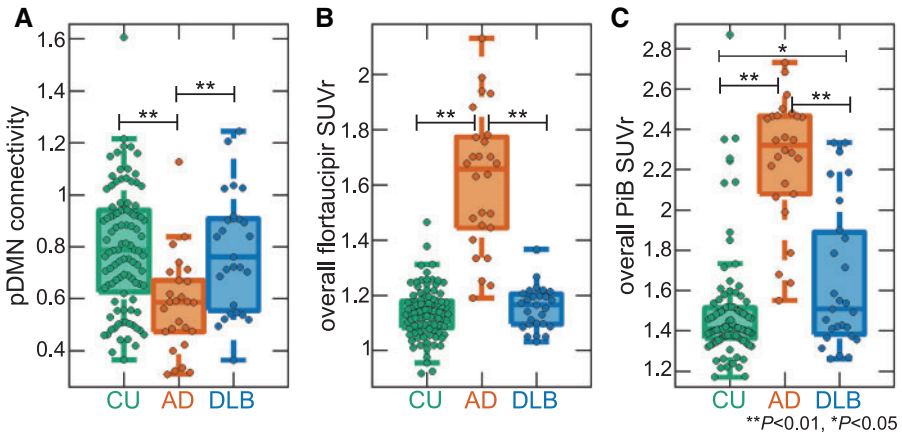

Figure 2 Group comparisons. (**A**) Group comparison of the posterior DMN connectivity between the three diagnostic groups. (**B**) Group comparison of overall flortaucipir SUVr between the three groups. (**C**) Group comparison of overall PiB SUVr between the three groups. Overall flortaucipir and PiB SUVr are estimated as the average flortaucipir SUVr from all cortical regions from the ADIR122 atlas. In each box plot, the central line corresponds to the sample median, the upper and lower border of the box represent the 25th and 75th percentile, respectively, and the length of the whiskers is 1.5 times the interquartile range. Posterior DMN connectivity and log-transformed flortaucipir and PiB SUVr were compared between the cognitively unimpaired (CU), Alzheimer's disease dementia (AD) and DLB groups using univariate ANOVAs with *post hoc* tests, Bonferroni-corrected for multiple comparisons.

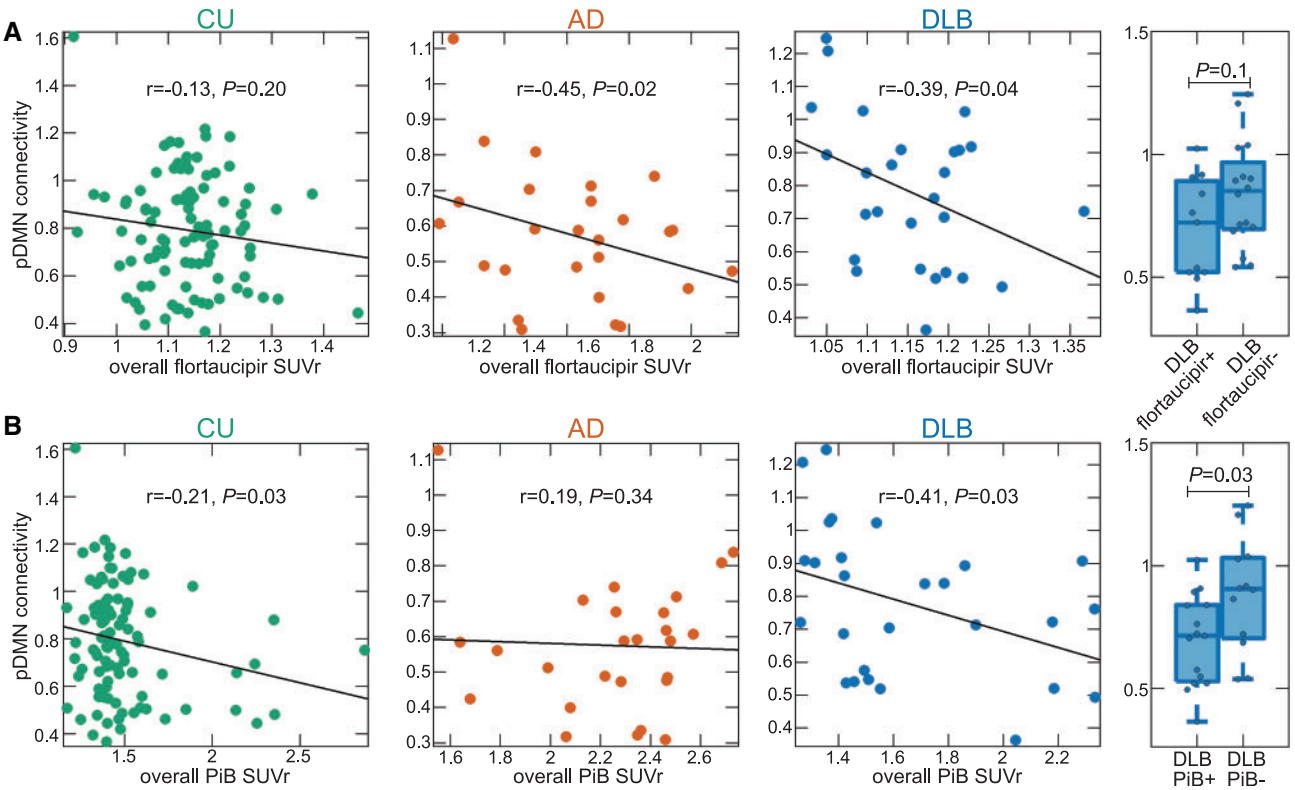

Figure 3 Association between DMN connectivity and flortaucipir uptake. (**A**) Pearson's correlation between overall flortaucipir SUVr (estimated from all cortical regions of the ADIR122 atlas) and posterior DMN connectivity in the three diagnostic groups and comparison of posterior DMN (pDMN) connectivity between DLB flortaucipir-positive and DLB flortaucipir-negative groups using a two-sample *t*-test. (**B**) Pearson's correlation between overall PiB SUVr and posterior DMN connectivity in the three diagnostic groups and comparison of posterior DMN connectivity between DLB PiB-positive and DLB PiB-negative groups using a two-sample *t*-test. AD = Alzheimer's disease; CU = cognitively unimpaired; flortaucipir+ = patients with DLB with global cortical flortaucipir SUVr $\geqslant$1.25; flortaucipir– = patients with DLB with global cortical flortaucipir SUVr $<$1.25; PiB+ = patients with DLB with global cortical PiB SUVr $\geqslant$1.48; PiB– = patients with DLB with global cortical PiB SUVr $<$1.48.

there was no significant correlation in the control group ($r = -0.13$, $P = 0.20$; Fig. 3A). Posterior DMN connectivity was not significantly different between flortaucipir-positive and -negative patients with DLB [$t(25) = 1.7$, $P = 0.10$].

Overall mean cortical PiB SUVr was significantly correlated with posterior DMN connectivity in the control group ($r = -0.21$, $P = 0.03$) and in the DLB group ($r = -0.41$, $P = 0.03$), but this correlation was not significant in the patients with Alzheimer's disease

Table 2 Mean and standard deviation of z-scores and goodness-of-fit values for each functional network in Alzheimer's disease dementia and DLB and results from one-sample t-tests

	Alzheimer's disease dementia		DLB	
	Mean (SD)	One-sample *t*-test (test value = 0)	Mean (SD)	One-sample *t*-test (test value = 0)
Z-score				
Dorsal attention network	8.0 (4.7)	$t(25) = 8.6$, $P < 0.001$	0.57 (0.9)	$t(26) = 3.2$, $P = 0.02$
Fronto-parietal network	7.9 (4.8)	$t(25) = 8.5$, $P < 0.001$	0.49 (1.0)	$t(26) = 2.5$, $P = 0.14$
Default mode network	7.0 (3.8)	$t(25) = 9.4$, $P < 0.001$	0.40 (1.2)	$t(26) = 1.8$, $P = 0.58$
Visual network	6.9 (5.8)	$t(25) = 6.1$, $P < 0.001$	0.38 (0.9)	$t(26) = 2.1$, $P = 0.30$
Limbic network	5.5 (2.5)	$t(25) = 11.2$, $P < 0.001$	0.24 (0.9)	$t(26) = 1.4$, $P = 1.0$
Ventral attention network	5.5 (3.6)	$t(25) = 7.8$, $P < 0.001$	0.09 (0.9)	$t(26) = 0.5$, $P = 1.0$
Somatomotor network	3.5 (3.3)	$t(25) = 5.4$, $P < 0.001$	–0.01 (0.7)	$t(26) = -0.06$, $P = 1.0$
Goodness-of-fit				
Dorsal attention network	1.9 (2.0)	$t(25) = 4.9$, $P < 0.001$	0.30 (0.33)	$t(26) = 4.7$, $P < 0.001$
Fronto-parietal network	1.9 (2.1)	$t(25) = 4.6$, $P < 0.001$	0.21 (0.35)	$t(26) = 3.1$, $P = 0.03$
Default mode network	0.7 (1.8)	$t(25) = 2.0$, $P = 0.38$	0.11 (0.50)	$t(26) = 1.1$, $P = 1.0$
Visual network	0.7 (4.6)	$t(25) = 0.8$, $P = 1.0$	0.08 (0.79)	$t(26) = 0.53$, $P = 1.0$
Limbic network	–0.9 (3.0)	$t(25) = -1.6$, $P = 0.92$	–0.08 (0.46)	$t(26) = -0.9$, $P = 1.0$
Ventral attention network	–1.0 (1.7)	$t(25) = -2.8$, $P = 0.06$	–0.26 (0.20)	$t(26) = -6.5$, $P < 0.001$
Somatomotor network	–3.3 (2.2)	$t(25) = -7.5$, $P < 0.001$	–0.37 (0.52)	$t(26) = -3.7$, $P = 0.007$

P-values are Bonferroni-corrected across the seven networks.

dementia ($r = -0.09$, $P = 0.67$, Fig. 3B). Posterior DMN connectivity was significantly lower in PiB-positive compared to PiB-negative patients with DLB [$t(25) = 2.3$, $P = 0.03$].

These results remained consistent when two-compartment partial volume correction[80] was applied to the flortaucipir and PiB PET images (Supplementary material).

Network-specificity of flortaucipir uptake

In the Alzheimer's disease dementia group, increased flortaucipir SUVr compared to control levels was observed for all seven networks, i.e. mean z-scores for each network were significantly different from zero ($P < 0.001$ for all networks; Table 2). In the DLB group, the only network that showed consistently higher flortaucipir uptake compared to control participants was the dorsal attention network ($P = 0.02$). However, flortaucipir uptake was not homogeneously distributed across all networks. The gradient of severity of flortaucipir uptake followed the same order in Alzheimer's disease dementia and DLB: dorsal attention network > fronto-parietal network > DMN > visual network > limbic network > ventral attention network > somatomotor network. In both Alzheimer's disease dementia and DLB, significant positive goodness-of-fit scores were only found for the fronto-parietal and the dorsal attention networks, indicating preferential flortaucipir uptake within these networks in relation to cortex-wide uptake (Table 2 and Fig. 4). These results remained consistent when using the 400 region parcellation (Supplementary Table 1). The pattern of network-specificity of flortaucipir uptake was similar in the DLB PiB-positive and DLB PiB-negative subgroups (Supplementary Fig. 1).

Association between functional connectivity and tau covariance

There was a significant association between higher group-average region-to-region functional connectivity and higher tau covariance in cognitively unimpaired ($\beta = 0.48$, $P < 0.001$), Alzheimer's disease dementia ($\beta = 0.66$, $P < 0.001$) and DLB ($\beta = 0.36$, $P < 0.001$; Fig. 5A). These associations remained significant when controlling for Euclidean distance between region centroids (cognitively unimpaired: $\beta = 0.34$, $P < 0.001$; Alzheimer's disease dementia: $\beta = 0.48$, $P < 0.001$; DLB: $\beta = 0.26$, $P < 0.001$). Controlling for distance between regions across the cortical surface instead led to very similar results (cognitively unimpaired: $\beta = 0.35$, $P < 0.001$; Alzheimer's disease dementia: $\beta = 0.48$, $P < 0.001$; DLB: $\beta = 0.27$, $P < 0.001$). There was a significant association between functional connectivity and tau covariance in the DLB PiB-positive ($\beta = 0.28$, $P < 0.001$) and DLB PiB-negative subgroups ($\beta = 0.32$, $P < 0.001$; Supplementary Fig. 2A).

Adjusting the tau covariance analysis for age and sex did not influence the results (cognitively unimpaired: $\beta = 0.50$, $P < 0.001$; Alzheimer's disease dementia: $\beta = 0.59$, $P < 0.001$; DLB: $\beta = 0.36$, $P < 0.001$).

Tau hot/cold spot analysis

For seed regions with high flortaucipir SUVr, higher functional connectivity of a target region to this seed region was associated with higher flortaucipir SUVr in the target region. In contrast, for seed regions with lower flortaucipir SUVrs, higher functional connectivity of a target region to this seed region was associated with lower flortaucipir SUVr in the target region (Fig. 5B). This was reflected in significant positive correlations between flortaucipir SUVr in the seed region and the association strength between seed-to-target functional connectivity with flortaucipir SUVr in the target region (β-values from linear regression) in cognitively unimpaired, Alzheimer's disease dementia and DLB (Fig. 5B). These results remained consistent when restricting the analysis to regions with flortaucipir SUVr >1.0 and >1.1 (Supplementary Fig. 3) and when using the 400 region parcellation (Supplementary material).

The region with highest average flortaucipir SUVr (tau hotspot) was located in the limbic network (left inferior/middle temporal gyrus) in all three groups whereas the region with lowest average flortaucipir SUVr (tau cold spot) was located within the somatomotor network (right insular/central opercular cortex) in all three groups (Supplementary Fig. 4).

Higher functional connectivity of a target region with the tau hotspot was associated with higher flortaucipir SUVr in the target region in all groups (Fig. 5C) whereas higher functional

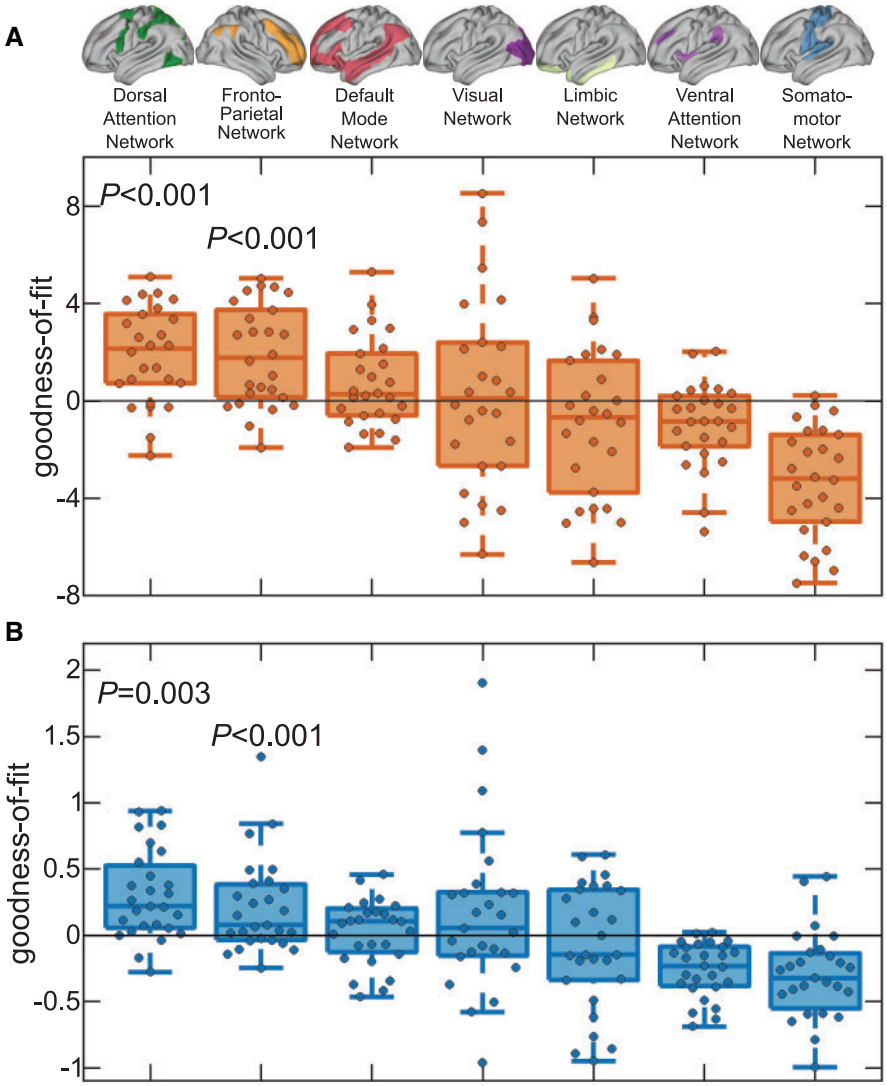

Figure 4 Network-specificity of flortaucipir uptake. Box plots of goodness-of-fit values assessing the network-specificity of flortaucipir uptake within seven functional networks from Yeo *et al.*[79] in the (**A**) Alzheimer's disease and (**B**) DLB groups. In each box plot, the central line corresponds to the sample median, the upper and lower border of the box represent the 25th and 75th percentile, respectively, and the length of the whiskers is 1.5 times the interquartile range. Significant *P*-values from one-sample *t*-tests (Bonferroni-corrected across the seven networks) are indicated, for all other networks *P*-values were >0.05 (see Table 2 for details on statistics).

connectivity of a target region with the tau cold spot was associated with lower flortaucipir SUVr in the target region in all groups (Fig. 5D).

Higher functional connectivity with tau hotspots was predictive of higher flortaucipir SUVr in a target region also on the individual participant level in DLB [$t(25) = 11.6$, $P < 0.001$]. Conversely, higher connectivity with tau cold spots was predictive of lower flortaucipir SUVr in a target region on the individual participant level in DLB [$t(25) = -10.8$, $P < 0.001$]. There were no differences in β-values between PiB-positive and -negative patients with DLB [hotspot: $t(25) = 1.1$, $P = 0.27$, cold spot: $t(25) = 0.5$, $P = 0.64$] or between patients with DLB who were *APOE* ε4 carriers and those who were not [hotspot: $t(25) = 0.8$, $P = 0.41$, cold spot: $t(25) = 1.4$, $P = 0.18$].

Repeating the hot and cold spot analysis separately in the DLB PiB-positive and DLB PiB-negative subgroups showed similar results (Supplementary Fig. 2). There was a significant positive correlation between flortaucipir SUVr in the seed region and the association strength of seed-to-target functional connectivity with flortaucipir SUVr in the target region in DLB PiB-positive ($r = 0.79$, $P < 0.001$) and DLB PiB-negative ($r = 0.78$, $P < 0.001$; Supplementary Fig. 2B). In both subgroups, the tau hotspot was located in left inferior/middle temporal gyrus and the tau cold spot was located in the somatomotor network. Higher functional connectivity of a target region with the tau hotspot was associated with higher flortaucipir SUVr in the target region in both subgroups (Supplementary Fig. 2C) whereas higher functional connectivity of a target region with the tau cold spot was associated with lower flortaucipir SUVr in the target region in both subgroups (Supplementary Fig. 2D).

Discussion

In this study, we investigated the relationship between functional network structure and the distribution of Alzheimer's disease pathology in patients with DLB from two different perspectives. In the first part, we showed that there is an association between greater overall amyloid and tau burden and a loss of posterior DMN connectivity in patients with DLB. In the second part, we found a relationship between the brain's functional network

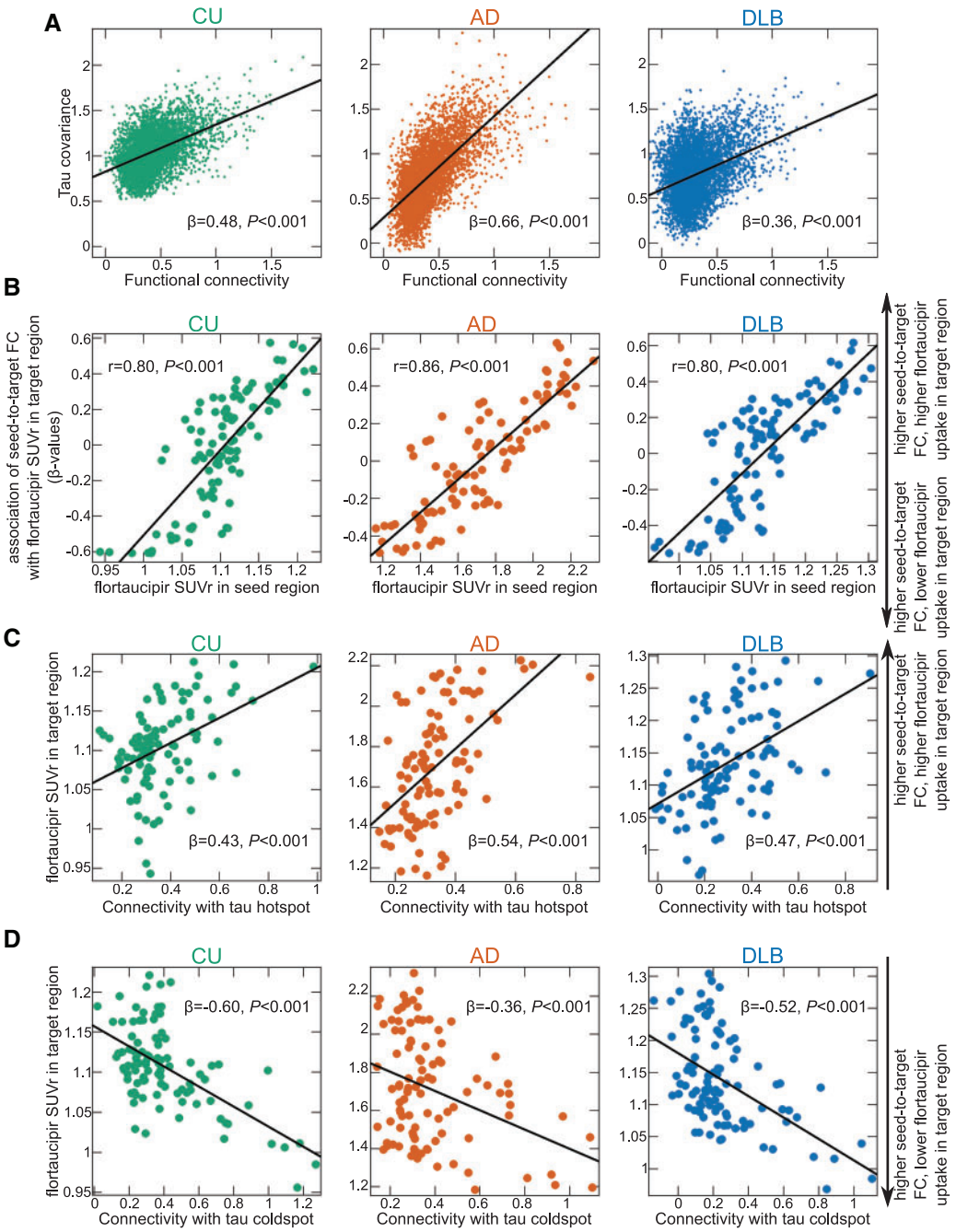

Figure 5 Association between functional connectivity and tau covariance. (**A**) Linear regression with the group-average functional connectivity matrix as the independent variable and the tau covariance matrix as the dependent variable in the three diagnostic groups. (**B**) Pearson's correlation between the association between seed-to-target functional connectivity with flortaucipir SUVr in the target region and flortaucipir SUVr in the seed region. Negative β-values (on the *y*-axis) indicate that higher seed-to-target connectivity is associated with lower flortaucipir uptake in the target region whereas positive β-values indicate that higher seed-to-target connectivity is associated with higher flortaucipir uptake in the target region. (**C**) Association between the strength of functional connectivity of a region with the tau hotspot (region with highest flortaucipir SUVr) and flortaucipir SUVr in that target region (linear regression). (**D**) Association between the strength of functional connectivity of a region with the tau cold spot (region with lowest flortaucipir SUVr) and flortaucipir SUVr in that target region (linear regression).

structure and the accumulation of tau pathology in Alzheimer's disease and DLB.

A decrease in posterior DMN connectivity is typical of Alzheimer's disease[37–40] and is thought to occur early in the course of the disease.[40,81–83] These DMN changes have been linked to the amount of tau and amyloid pathology in the brain not only in patients with Alzheimer's disease, but also in asymptomatic individuals.[33,41,42] In DLB, however, DMN findings from different studies are much less consistent and it is still debated whether DMN changes are a feature of Lewy body dementias.[46–48] In the present study, we found a significant reduction in posterior DMN connectivity in the Alzheimer's disease group compared to control participants and patients with DLB, whereas posterior DMN connectivity in the DLB group was not different from healthy control levels.

Nevertheless, the DLB group showed a correlation between higher overall tau and amyloid burden and a reduction in posterior

DMN connectivity. Furthermore, DMN connectivity was significantly reduced in PiB-positive compared to PiB-negative patients with DLB and a similar trend was observed for flortaucipir-positive compared to flortaucipir-negative patients with DLB. These findings indicate that patients with DLB with more concurrent Alzheimer's disease pathology show a more severe loss of DMN connectivity, i.e. a higher burden of Alzheimer's disease pathology is linked to a more Alzheimer's disease-like functional connectivity pattern in patients with DLB. This extends previous studies that have linked concurrent Alzheimer's disease pathology in patients with DLB to a more Alzheimer's disease-like clinical presentation[16,84] and more Alzheimer's disease-like atrophy patterns.[10,12,13] Furthermore, the results indicate that DMN changes in patients with DLB might be driven more by Alzheimer's disease than by Lewy body pathology. This in turn might explain inconsistencies in previous DLB studies with respect to DMN connectivity as these studies typically did not assess the amount of concurrent Alzheimer's disease pathology in their cohorts.

In the Alzheimer's disease group, posterior DMN connectivity was correlated with overall flortaucipir SUVr, but not with PiB SUVr. This is in line with observations from previous studies suggesting that tau pathology is more strongly related to neuronal dysfunction in patients with Alzheimer's disease than amyloid.[85,86] The present results indicate that neuronal changes underlying impaired DMN connectivity are also more strongly influenced by tau than by amyloid pathology in patients with Alzheimer's disease. In contrast, in the DLB group which included more people with low amyloid burden, i.e. who were at an earlier stage of the Alzheimer's disease pathology spectrum, the presence and severity of amyloid pathology still appears to have a more pronounced effect on posterior DMN connectivity.

In the second part, we investigated the association between tau deposition and the spatial extent of functional brain networks in Alzheimer's disease and patients with DLB. As expected, there was a consistent brain-wide increase in uptake of flortaucipir in Alzheimer's disease compared to control participants across all functional networks.[28] In contrast, the only network that showed increased flortaucipir uptake in DLB compared to control participants was the dorsal attention network, which includes parietal and posterior brain regions[9] that are also prone to disruption of structural connectivity in DLB.[87] When analysing the network-specificity of flortaucipir uptake, it became evident that tau pathology was not distributed homogeneously across the different networks. In contrast, we found a gradient of severity of flortaucipir uptake that was strikingly similar in Alzheimer's disease and DLB. In both groups, the only networks that showed significant preferential flortaucipir uptake compared to cortex-wide uptake were the dorsal attention and fronto-parietal networks. This is in line with previous studies in Alzheimer's disease showing that, compared to healthy control participants, tau deposition occurs preferentially within higher-order cognitive instead of primary sensory networks.[28,88] Even though the temporal progression of tau accumulation in patients with DLB often does not follow the typical Braak-type pattern observed in Alzheimer's disease,[21,89] the present findings suggest that the relationship between tau deposition and functional network structure appears to be similar in the two dementia groups.

Finally, when assessing the relationship between the distribution of tau pathology and functional connectivity between brain regions, we found that regions that are more strongly functionally connected with each other showed greater similarity (i.e. covariance) in flortaucipir uptake. This association was observed in all three diagnostic groups and was independent of PiB or *APOE* ε4 carrier status in the DLB group. Furthermore, this relationship remained significant after controlling for spatial proximity between regions, indicating that similarity in tau levels between regions cannot be fully explained by a model that simply relies on diffusion to spatially adjacent regions. This is in line with findings from previous animal and human studies in Alzheimer's disease and supports the notion that functional connectivity plays an important role in predicting regional tau burden.[54,55,57,90]

The tau hotspot, i.e. the region with highest flortaucipir uptake, was located in the inferior/middle temporal gyrus in all three groups whereas the tau cold spot was located within the somatomotor network, consistent with previous studies of tau distribution.[9,24,91] Regions that were more strongly connected to the tau hotspot also exhibited higher flortaucipir uptake themselves. Similarly, there was a linear relationship between higher connectivity of a region to the tau cold spot and lower tau levels in that region. This indicates that the level of tau pathology in a given region depends on its functional connectivity profile and suggests that tau pathology might be spreading through functional brain networks.[57,90,92] Additionally, it shows that the amount of tau spreading might depend on the strength of inter-regional functional connectivity, which is in line with previous *in vitro* and animal research indicating that the propagation of tau depends on the activity levels of synapses.[93,94]

Overall, these results are consistent with the trans-neuronal model of tau spreading. The results in our Alzheimer's disease group replicate previous findings from an independent cohort[57] and we show that there is a similar relationship between the distribution of tau pathology and the brain's functional network architecture in patients with DLB, independent of the amount of amyloid pathology. However, another explanation for the observed cross-sectional association between tau distribution and functional networks is that, instead of spreading from one area to another, tau could arise simultaneously throughout different areas belonging to the same functional network, which might be due to poor resilience to failure or lack of regional trophic support.[26,43] It is also possible that a combination of trans-neuronal spread and local network failure underlies the observed tau distribution patterns and future longitudinal analyses will help elucidate these mechanisms.

While Alzheimer's disease pathology plays an important role in the pathogenesis and clinical presentation of DLB, the hallmark pathology of DLB is α-synuclein for which the first PET tracers are currently being developed.[95] Findings from animal studies suggest that α-synuclein might also spread from neuron to neuron in a prion-like manner.[96–98] The analyses and results presented in this study will therefore pave the way for analysing the relationship between the distribution of α-synuclein pathology and functional network structure when an α-synuclein PET tracer becomes available. This will also shed light on potential synergistic mechanisms in the spread of Alzheimer's disease and Lewy body pathology[6,99,100] and how these relate to the brain's functional network structure.

Limitations

The flortaucipir PET ligand has been shown to exhibit off-target binding in areas such as the choroid plexus, which can influence measurements in the hippocampus, and the basal ganglia.[101] These areas of potential off-target binding are not part of the Schaefer atlas[67] and were therefore excluded from the present analysis. However, given the importance of structures such as the hippocampus and the basal ganglia in the context of Alzheimer's disease and DLB, it will be important to replicate the present analysis using novel tau-PET ligands that show less off-target binding,[102] which will allow inclusion of these regions. Second, the data used in this study are cross-sectional and the analyses are correlational. We can therefore only draw limited conclusions about the temporal progression of tau spreading in the brain.

Future longitudinal studies are needed to address this issue. Another potential limitation is the fact that most of our patients with DLB were male, which is due to the fact that DLB is more common in males than in females[103] and is therefore an inherent problem of many DLB studies. While we ensured that the proportion of males was matched in all three groups, there might be sex differences in the likelihood and regional distribution of coexisting Alzheimer's disease pathology in DLB that could not be investigated in the present study.[20]

Conclusion

In conclusion, this study showed that a higher burden of Alzheimer's disease co-pathology in patients with DLB is related to more Alzheimer's disease-like changes in functional connectivity. Furthermore, we found that the association between the brain's functional network structure and the propagation of tau pathology that has recently been described in Alzheimer's disease, is similarly present in patients with DLB, indicating that similar mechanisms of connectivity-related occurrence of tau pathology might be at work in both diseases.

Funding

This research was supported by the National Institutes of Health, US (R01 AG040042, R01 AG11378, P50 AG16574, U01 AG06786, and C06 RR018898), Foundation Dr Corinne Schulerand, the Mangurian Foundation for Lewy Body Research, The Elsie and Marvin Dekelboum Family Foundation and the Robert H. and Clarice Smith and Abigail Van Buren Alzheimer's Disease Research Program, by National Institute for Health Research (NIHR) Newcastle Biomedical Research Centre (BRC) based at Newcastle upon Tyne Hospitals NHS Foundation Trust and Newcastle University, and by Alzheimer's Research UK.

Competing interests

The authors report no competing interests.

Supplementary material

Supplementary material is available at *Brain* online.

References

1. McKeith I, O'Brien J, Walker Z, et al.; DLB Study Group. Sensitivity and specificity of dopamine transporter imaging with 123I-FP-CIT SPECT in dementia with Lewy bodies: A phase III, multicentre study. *Lancet Neurol*. 2007;6(4):305–313.
2. McKeith IG, Boeve BF, Dickson DW, et al. Diagnosis and management of dementia with Lewy bodies Fourth consensus report of the DLB Consortium. *Neurology*. 2017;89(1):88–100.
3. Dickson DW. Dementia with Lewy bodies: Neuropathology. *J Geriatr Psychiatry Neurol*. 2002;15(4):210–216.
4. McKeith IG, Dickson DW, Lowe J, et al.; Consortium on DLB. Diagnosis and management of dementia with Lewy bodies: Third report of the DLB consortium. *Neurology*. 2005;65(12):1863–1872.
5. Dugger BN, Adler CH, Shill HA, et al.; Arizona Parkinson's Disease Consortium. Concomitant pathologies among a spectrum of Parkinsonian disorders. *Parkinsonism Relat Disord*. 2014;20(5):525–529.
6. Howlett DR, Whitfield D, Johnson M, et al. Regional multiple pathology scores are associated with cognitive decline in Lewy body dementias. *Brain Pathol*. 2015;25(4):401–408.
7. Jellinger KA, Attems J. Prevalence and impact of vascular and Alzheimer pathologies in Lewy body disease. *Acta Neuropathol*. 2008;115(4):427–436.
8. Gomperts SN, Locascio JJ, Makaretz SJ, et al. Tau positron emission tomographic imaging in the Lewy body diseases. *JAMA Neurol*. 2016;73(11):1334–1341.
9. Kantarci K, Lowe VJ, Boeve BF, et al. AV-1451 tau and β-amyloid positron emission tomography imaging in dementia with Lewy bodies. *Ann Neurol*. 2017;81(1):58–67.
10. Nedelska Z, Ferman TJ, Boeve BF, et al. Pattern of brain atrophy rates in autopsy-confirmed dementia with Lewy bodies. *Neurobiol Aging*. 2015;36(1):452–461.
11. Sarro L, Senjem ML, Lundt ES, et al. Amyloid-β deposition and regional grey matter atrophy rates in dementia with Lewy bodies. *Brain*. 2016;139(10):2740–2750.
12. Shimada H, Shinotoh H, Hirano S, et al. β-Amyloid in Lewy body disease is related to Alzheimer's disease-like atrophy. *Mov Disord*. 2013;28(2):169–175.
13. van der Zande JJ, Steenwijk MD, ten Kate M, Wattjes MP, Scheltens P, Lemstra AW. Gray matter atrophy in dementia with Lewy bodies with and without concomitant Alzheimer pathology. *Neurobiol Aging*. 2018;71:171–178.
14. van Steenoven I, Aarsland D, Weintraub D, et al.; European DLB consortium. Cerebrospinal fluid Alzheimer's disease biomarkers across the spectrum of Lewy body diseases: results from a large multicenter cohort. *J Alzheimer's Dis*. 2016;54(1):287–295.
15. Graff-Radford J, Lesnick TG, Boeve BF, et al. Predicting survival in dementia with Lewy bodies with hippocampal volumetry. *Mov Disord*. 2016;31(7):989–994.
16. Lemstra AW, de Beer MH, Teunissen CE, et al. Concomitant AD pathology affects clinical manifestation and survival in dementia with Lewy bodies. *J Neurol Neurosurg Psychiatry*. 2017;88(2):113–118.
17. Foster ER, Campbell MC, Burack MA, et al. Amyloid imaging of Lewy body-associated disorders. *Mov Disord*. 2010;25(15):2516–2523.
18. Blanc F, Mahmoudi R, Jonveaux T, et al. Long-term cognitive outcome of Alzheimer's disease and dementia with Lewy bodies: Dual disease is worse. *Alzheimers Res Ther*. 2017;9(1):47.
19. Kraybill ML, Larson EB, Tsuang DW, et al. Cognitive differences in dementia patients with autopsy-verified AD, Lewy body pathology, or both. *Neurology*. 2005;64(12):2069–2073.
20. Ferman TJ, Aoki N, Boeve BF, et al. Subtypes of dementia with Lewy bodies are associated with α-synuclein and tau distribution. *Neurology*. 2020;95(2):e155–e165.
21. Braak H, Braak E. Neuropathological stageing of Alzheimer-related changes. *Acta Neuropathol*. 1991;82(4):239–259.
22. Braak H, Alafuzoff I, Arzberger T, Kretzschmar H, Del Tredici K. Staging of Alzheimer disease-associated neurofibrillary pathology using paraffin sections and immunocytochemistry. *Acta Neuropathol*. 2006;112(4):389–404.
23. Cho H, Choi JY, Hwang MS, et al. In vivo cortical spreading pattern of tau and amyloid in the Alzheimer disease spectrum. *Ann Neurol*. 2016;80(2):247–258.
24. Schöll M, Lockhart SN, Schonhaut DR, et al. PET imaging of Tau deposition in the aging human brain. *Neuron*. 2016;89(5):971–982.
25. Schwarz AJ, Yu P, Miller BB, et al. Regional profiles of the candidate tau PET ligand 18 F-AV-1451 recapitulate key features of Braak histopathological stages. *Brain*. 2016;139(Pt 5):1539–1550.

26. Jones DT, Graff-Radford J, Lowe VJ, et al. Tau, amyloid, and cascading network failure across the Alzheimer's disease spectrum. *Cortex*. 2017;97:143–159.
27. Hoenig MC, Bischof GN, Seemiller J, et al. Networks of tau distribution in Alzheimer's disease. *Brain*. 2018;141(2):568–581.
28. Hansson O, Grothe MJ, Strandberg TO, et al. Tau pathology distribution in Alzheimer's disease corresponds differentially to cognition-relevant functional brain networks. *Front Neurosci*. 2017;11:167.
29. Ossenkoppele R, Iaccarino L, Schonhaut DR, et al. Tau covariance patterns in Alzheimer's disease patients match intrinsic connectivity networks in the healthy brain. *NeuroImage Clin*. 2019;23:101848.
30. Grothe MJ, Teipel SJ., Alzheimer's Disease Neuroimaging Initiative. Spatial patterns of atrophy, hypometabolism, and amyloid deposition in Alzheimer's disease correspond to dissociable functional brain networks. *Hum Brain Mapp*. 2016;37(1):35–53.
31. Mormino EC, Smiljic A, Hayenga AO, et al. Relationships between beta-amyloid and functional connectivity in different components of the default mode network in aging. *Cereb Cortex*. 2011;21(10):2399–2407.
32. Buckner RL, Sepulcre J, Talukdar T, et al. Cortical hubs revealed by intrinsic functional connectivity: Mapping, assessment of stability, and relation to Alzheimer's disease. *J Neurosci*. 2009;29(6):1860–1873.
33. Palmqvist S, Schöll M, Strandberg O, et al. Earliest accumulation of β-amyloid occurs within the default-mode network and concurrently affects brain connectivity. *Nat Commun*. 2017;8(1):1214.
34. Sperling RA, Laviolette PS, O'Keefe K, et al. Amyloid deposition is associated with impaired default network function in older persons without dementia. *Neuron*. 2009;63(2):178–188.
35. Raichle ME, Macleod AM, Snyder AZ, et al. A default mode of brain function. Proc Natl Acad Sci U S A. 2001;98(2):676–682.
36. Fox MD, Snyder AZ, Vincent JL, Corbetta M, Van Essen DC, Raichle ME. The human brain is intrinsically organized into dynamic, anticorrelated functional networks. *Proc Natl Acad Sci U S A*. 2005;102(27):9673–9678.
37. Badhwar A, Tam A, Dansereau C, Orban P, Hoffstaedter F, Bellec P. Resting-state network dysfunction in Alzheimer's disease: A systematic review and meta-analysis. *Alzheimer's Dement*. 2017;8(1):73–85.
38. Greicius MD, Srivastava G, Reiss AL, Menon V. Default-mode network activity distinguishes Alzheimer's disease from healthy aging: Evidence from functional MRI. *Proc Natl Acad Sci U S A*. 2004;101(13):4637–4642.
39. Jones DT, Machulda MM, Vemuri P, et al. Age-related changes in the default mode network are more advanced in Alzheimer disease. *Neurology*. 2011;77(16):1524–1531.
40. Binnewijzend MAA, Schoonheim MM, Sanz-Arigita E, et al. Resting-state fMRI changes in Alzheimer's disease and mild cognitive impairment. *Neurobiol Aging*. 2012;33(9):2018–2028.
41. Schultz AP, Chhatwal JP, Hedden T, et al. Phases of hyperconnectivity and hypoconnectivity in the default mode and salience networks track with amyloid and tau in clinically normal individuals. *J Neurosci*. 2017;37(16):4323–4331.
42. Sheline YI, Raichle ME, Snyder AZ, et al. Amyloid plaques disrupt resting state default mode network connectivity in cognitively normal elderly. *Biol Psychiatry*. 2010;67(6):584–587.
43. Jones DT, Knopman DS, Gunter JL, et al.; Alzheimer's Disease Neuroimaging Initiative. Cascading network failure across the Alzheimer's disease spectrum. *Brain*. 2016;139(Pt 2):547–562.
44. Kenny ER, Blamire AM, Firbank MJ, O'Brien JT. Functional connectivity in cortical regions in dementia with Lewy bodies and Alzheimer's disease. *Brain*. 2012;135(Pt 2):569–581.
45. Lowther ER, O'Brien JT, Firbank MJ, Blamire AM. Lewy body compared with Alzheimer dementia is associated with decreased functional connectivity in resting state networks. *Psychiatry Res Neuroimaging*. 2014;223(3):192–201.
46. Franciotti R, Falasca NW, Bonanni L, et al. Default network is not hypoactive in dementia with fluctuating cognition: An Alzheimer disease/dementia with Lewy bodies comparison. *Neurobiol Aging*. 2013;34(4):1148–1158.
47. Peraza LR, Kaiser M, Firbank MJ, et al. fMRI resting state networks and their association with cognitive fluctuations in dementia with Lewy bodies. *NeuroImage Clin*. 2014;4:558–565.
48. Schumacher J, Peraza LR, Firbank MJ, et al. Functional connectivity in dementia with Lewy bodies: A within- and between-network analysis. *Hum Brain Mapp*. 2018;39(3):1118–1129.
49. Galvin JE, Price JL, Yan Z, Morris JC, Sheline YI. Resting bold fMRI differentiates dementia with Lewy bodies vs Alzheimer disease. *Neurology*. 2011;76(21):1797–1803.
50. Frost B, Diamond MI. Prion-like mechanisms in neurodegenerative diseases. *Nat Rev Neurosci*. 2010;11(3):155–159.
51. Brettschneider J, Tredici K, Del Lee VMY, Trojanowski JQ. Spreading of pathology in neurodegenerative diseases: A focus on human studies. *Nat Rev Neurosci*. 2015;16(2):109–120.
52. Walsh DM, Selkoe DJ. A critical appraisal of the pathogenic protein spread hypothesis of neurodegeneration. *Nat Rev Neurosci*. 2016;17(4):251–260.
53. Clavaguera F, Hench J, Goedert M, Tolnay M. Invited review: Prion-like transmission and spreading of tau pathology. *Neuropathol Appl Neurobiol*. 2015;41(1):47–58.
54. de Calignon A, Polydoro M, Suárez-Calvet M, et al. Propagation of tau pathology in a model of early Alzheimer's disease. *Neuron*. 2012;73(4):685–697.
55. Liu L, Drouet V, Wu JW, et al. Trans-synaptic spread of tau pathology in vivo. *PLoS ONE*. 2012;7(2):e31302.
56. Cope TE, Rittman T, Borchert RJ, et al. Tau burden and the functional connectome in Alzheimer's disease and progressive supranuclear palsy. *Brain*. 2018;141(2):550–567.
57. Franzmeier N, Rubinski A, Neitzel J, et al.; Alzheimer's Disease Neuroimaging Initiative. Functional connectivity associated with tau levels in ageing, Alzheimer's, and small vessel disease. *Brain*. 2019;142(4):1093–1107.
58. Vogel JW, Iturria-Medina Y, Strandberg OT, Smith R, Evans AC, Hansson O. Spread of pathological tau proteins through communicating neurons in human Alzheimer's disease. *bioRxiv*. [Preprint] doi:10.1101/555821
59. Franzmeier N, Neitzel J, Rubinski A, et al.; Alzheimer's Disease Neuroimaging Initiative (ADNI). Functional brain architecture is associated with the rate of tau accumulation in Alzheimer's disease. *Nat Commun*. 2020;11(1):347.
60. McKhann GM, Knopman DS, Chertkow H, et al. The diagnosis of dementia due to Alzheimer's disease: Recommendations from the National Institute on Aging-Alzheimer's Association workgroups on diagnostic guidelines for Alzheimer's disease. *Alzheimer's Dement*. 2011;7(3):263–269.
61. Ferman TJ, Smith GE, Boeve BF, et al. DLB fluctuations: Specific features that reliably differentiate DLB from AD and normal aging. *Neurology*. 2004;62(2):181–187.
62. Boeve BF, Molano JR, Ferman TJ, et al. Validation of the Mayo Sleep Questionnaire to screen for REM sleep behavior disorder in an aging and dementia cohort. *Sleep Med*. 2011;12(5):445–453.
63. Schwarz CG, Gunter JL, Lowe VJ, et al. A comparison of partial volume correction techniques for measuring change in serial amyloid PET SUVR. *J Alzheimer's Dis*. 2019;67(1):181–195.
64. Ashburner J, Friston KJ. Unified segmentation. *Neuroimage*. 2005;26(3):839–851.

65. Schwarz CG, Gunter JL, Ward CP, et al. The Mayo clinic adult lifespan template: better quantification across the lifespan. *Alzheimer's Dement*. 2017;13:P792. doi:10.1016/j.jalz.2017.06.1071
66. Avants BB, Epstein CL, Grossman M, Gee JC. Symmetric diffeomorphic image registration with cross-correlation: Evaluating automated labeling of elderly and neurodegenerative brain. *Med Image Anal*. 2008;12(1):26–41.
67. Schaefer A, Kong R, Gordon EM, et al. Local-global parcellation of the human cerebral cortex from intrinsic functional connectivity MRI. *Cereb Cortex*. 2018;28(9):3095–3114.
68. Jack CR, Wiste HJ, Weigand SD, et al. Defining imaging biomarker cut points for brain aging and Alzheimer's disease. *Alzheimer's Dement*. 2017;13(3):205–216.
69. Lowe VJ, Bruinsma TJ, Wiste HJ, et al. Cross-sectional associations of tau-PET signal with cognition in cognitively unimpaired adults. *Neurology*. 2019;93(1):e29–e39.
70. Cox RW. AFNI: Software for analysis and visualization of functional magnetic resonance neuroimages. *Comput Biomed Res*. 1996;29(3):162–173.
71. Behzadi Y, Restom K, Liau J, Liu TT. A component based noise correction method (CompCor) for BOLD and perfusion based fMRI. *Neuroimage*. 2007;37(1):90–101.
72. Hallquist MN, Hwang K, Luna B. The nuisance of nuisance regression: Spectral misspecification in a common approach to resting-state fMRI preprocessing reintroduces noise and obscures functional connectivity. *Neuroimage*. 2013;82:208–225.
73. Wiepert DA, Lowe VJ, Knopman DS, et al. A robust biomarker of large-scale network failure in Alzheimer's disease. *Alzheimers Dement (Amst)*. 2017;6:152–161.
74. Jones DT, Vemuri P, Murphy MC, et al. Non-stationarity in the 'Resting Brain's' modular architecture. *PLoS Biol*. 2012;7(6):e39731.
75. Calhoun VD, Adali T, Pearlson GD, Pekar JJ. A method for making group inferences from functional MRI data using independent component analysis. *Hum Brain Mapp*. 2001;14(3):140–151.
76. Alexander-Bloch A, Raznahan A, Bullmore E, Giedd J. The convergence of maturational change and structural covariance in human cortical networks. *J Neurosci*. 2013;33(7):2889–2899.
77. Hafkemeijer A, Möller C, Dopper EGP, et al. Differences in structural covariance brain networks between behavioral variant frontotemporal dementia and Alzheimer's disease. *Hum Brain Mapp*. 2016;37(3):978–988.
78. Di X, Biswal BB., Alzheimer's Disease Neuroimaging Initiative. Metabolic brain covariant networks as revealed by FDG-PET with reference to resting-state fMRI networks. *Brain Connect*. 2012;2(5):275–283.
79. Yeo BT, Krienen FM, Sepulcre J, et al. The organization of the human cerebral cortex estimated by intrinsic functional connectivity. *J Neurophysiol*. 2011;106(3):1125–1165.
80. Meltzer CC, Leal JP, Mayberg HS, Wagner HN, Frost JJ. Correction of PET data for partial volume effects in human cerebral cortex by MR imaging. *J Comput Assist Tomogr*. 1990;14(4):561–570.
81. Damoiseaux JS, Prater KE, Miller BL, Greicius MD. Functional connectivity tracks clinical deterioration in Alzheimer's disease. *Neurobiol Aging*. 2012;33(4):828.e19-828–e30.
82. Sheline YI, Morris JC, Snyder AZ, et al. APOE4 allele disrupts resting state fMRI connectivity in the absence of amyloid plaques or decreased CSF A 42. *J Neurosci*. 2010;30(50):17035–17040.
83. Patel KT, Stevens MC, Pearlson GD, et al. Default mode network activity and white matter integrity in healthy middle-aged ApoE4 carriers. *Brain Imaging Behav*. 2013;7(1):60–67.
84. Merdes AR, Hansen LA, Jeste DV, et al. Influence of Alzheimer pathology on clinical diagnostic accuracy in dementia with Lewy bodies. *Neurology*. 2003;60(10):1586–1590.
85. Jack CR, Knopman DS, Jagust WJ, et al. Hypothetical model of dynamic biomarkers of the Alzheimer's pathological cascade. *Lancet Neurol*. 2010;9(1):119–128.
86. Whitwell JL, Dickson DW, Murray ME, et al. Neuroimaging correlates of pathologically defined subtypes of Alzheimer's disease: A case-control study. *Lancet Neurol*. 2012;11(10):868–877.
87. Nedelska Z, Schwarz CG, Boeve BF, et al. White matter integrity in dementia with Lewy bodies: A voxel-based analysis of diffusion tensor imaging. *Neurobiol Aging*. 2015;36(6):2010–2017.
88. Pereira JB, Ossenkoppele R, Palmqvist S, et al. Amyloid and tau accumulate across distinct spatial networks and are differentially associated with brain connectivity. *eLife*. 2019;8:e50830.
89. Walker L, McAleese KE, Thomas AJ, et al. Neuropathologically mixed Alzheimer's and Lewy body disease: Burden of pathological protein aggregates differs between clinical phenotypes. *Acta Neuropathol*. 2015;129(5):729–748.
90. Vogel JW, Iturria-Medina Y, Strandberg OT, et al. Swedish BioFinder Study. Spread of pathological tau proteins through communicating neurons in human Alzheimer's disease. *Nat Commun*. 2020;11(1):2612.
91. Jack CR, Wiste HJ, Schwarz CG, et al. Longitudinal tau PET in ageing and Alzheimer's disease. *Brain*. 2018;141(5):1517–1528.
92. Adams JN, Maass A, Harrison TM, Baker SL, Jagust WJ. Cortical tau deposition follows patterns of entorhinal functional connectivity in aging. *eLife*. 2019;8:e49132.
93. Wu JW, Hussaini SA, Bastille IM, et al. Neuronal activity enhances tau propagation and tau pathology in vivo. *Nat Neurosci*. 2016;19(8):1085–1092.
94. Pooler AM, Phillips EC, Lau DHW, Noble W, Hanger DP. Physiological release of endogenous tau is stimulated by neuronal activity. *EMBO Rep*. 2013;14(4):389–394.
95. Maurer A, Leonov A, Ryazanov S, et al. 11 C Radiolabeling of anle253b: A putative PET tracer for Parkinson's disease that binds to α-Synuclein fibrils in vitro and crosses the blood-brain barrier. *ChemMedChem*. 2020;15(5):411–415.
96. Dehay B, Vila M, Bezard E, Brundin P, Kordower JH. Alpha-synuclein propagation: New insights from animal models. *Mov Disord*. 2016;31(2):161–168.
97. Henderson MX, Trojanowski JQ, Lee VMY. α-Synuclein pathology in Parkinson's disease and related α-synucleinopathies. *Neurosci Lett*. 2019;709:134316.
98. Steiner JA, Quansah E, Brundin P. The concept of alpha-synuclein as a prion-like protein: Ten years after. *Cell Tissue Res*. 2018;373(1):161–173.
99. Pletnikova O, West N, Lee MK, et al. Aβ deposition is associated with enhanced cortical α-synuclein lesions in Lewy body diseases. *Neurobiol Aging*. 2005;26(8):1183–1192.
100. Bassil F, Brown HJ, Pattabhiraman S, et al. Amyloid-beta (Aβ) plaques promote seeding and spreading of alpha-synuclein and tau in a mouse model of Lewy body disorders with Aβ pathology. *Neuron*. 2020;105(2):260–275.e6.
101. Marquié M, Verwer EE, Meltzer AC, et al. Lessons learned about [F-18]-AV-1451 off-target binding from an autopsy-confirmed Parkinson's case. *Acta Neuropathol Commun*. 2017;5(1):75.
102. Wong DF, Comley RA, Kuwabara H, et al. Characterization of 3 novel tau radiopharmaceuticals, 11 C-RO-963, 11 C-RO-643, and 18 F-RO-948, in healthy controls and in Alzheimer subjects. *J Nucl Med*. 2018;59(12):1869–1876.
103. Savica R, Grossardt BR, Bower JH, Boeve BF, Ahlskog JE, Rocca WA. Incidence of dementia with Lewy bodies and Parkinson disease dementia. *JAMA Neurol*. 2013;70(11):1396–1402.